

Pseudospin 3/2 Fermions, Type-II Weyl Semimetals and Critical Weyl Semimetals in Tricolor Cubic Lattice

Motohiko Ezawa

Department of Applied Physics, University of Tokyo, Hongo 7-3-1, 113-8656, Japan

Multi-band touchings such as 3-band, 6-band and 8-band touchings together with the emergence of high pseudospin fermions were predicted recently at high-symmetry points in three-dimensional space. In this paper, we propose a simple cubic model whose unit cell contains three atoms. There are 6 bands in the system due to the spin degrees of freedom. The 4-band and 2-band touchings are realized at high-symmetry points, where we derive low-energy theories, demonstrating the emergence of pseudospin-3/2 fermions and Weyl fermions, respectively. Away from the high-symmetry points, we find critical Weyl fermions present exactly at the boundary between the type-I and type-II Weyl fermions. This critical Weyl fermion transforms into the type-I or type-II Weyl fermion once the magnetic field is applied.

Dirac, Weyl and Majorana fermions have attracted much attention in condensed matter physics in views of topology and symmetry. They have a 2-band touching with a linear dispersion. Dirac and Weyl fermions emerge in various materials, which are called Dirac and Weyl semimetals¹. An interesting feature of Weyl semimetals is that they have a monopole charge in the momentum space, which protects the existence of the Weyl points topologically². The type-II Weyl semimetal has attracted much attention recently^{3–12}, which emerges when the Weyl cone is highly tilted so that the Fermi surface consists of a pair of electron- and hole- pockets touching at the Weyl point. It is experimentally realized in MoTe_2 ^{13–17}, LaAlGe ¹⁸, WTe_2 ^{19–22}, TaIrTe_4 ²³, PtTe_2 ²⁴ and Ta_3S_2 ²⁵.

Very recently, new types of fermions with multi-band touching were proposed based on the symmetry analysis as well as the first-principles calculations, where 3-band^{26,27}, 6-band²⁶ and 8-band^{26,28} touchings were reported at high-symmetry points. Especially, it is shown that the 3-band touchings are well described by the fermions carrying the pseudospin 1. Furthermore, the 8-band touching has been proposed in antiperovskites to produce a pseudospin-3/2 fermion²⁹. On the other hand, the 4-band touching is yet to be realized although some discussions were given in the supplement of Ref.²⁶.

In this paper, motivated by these proposals on multi-band touchings and fermions carrying higher pseudospins, we present tight-binding models possessing 4-band and 2-band touchings [Fig.1]. They are realized naturally in a lattice structure with the cubic symmetry where the unit cell contains three atoms [Fig.2]. We call it a tricolor cubic lattice. First, we derive the low-energy 4-band theory at the high-symmetry points, which is shown to produce pseudospin-3/2 fermions having the angular momenta $j = (-3/2, -1/2, 1/2, 3/2)$. We also show that the bands have monopole charges $-3, -1, 1, 3$ at these points. Second, the 2-band theory is described by the Weyl fermion. Furthermore, away from the high-symmetry points, we find a critical Weyl fermion, which resides at the exact boundary of the type-I and type-II Weyl fermions. They transform into the type-I or type-II Weyl fermions once the magnetic field is applied.

Tricolor cubic lattice: We consider a cubic lattice as illustrated in Fig.2(a). Though it looks complicated, the unit cell is

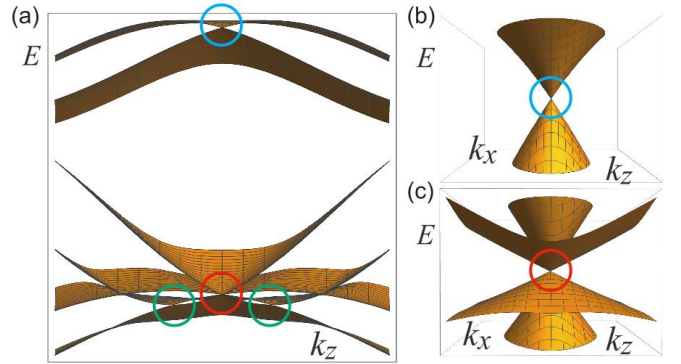


FIG. 1: Bird's eye's view of the band structure near the P point. The horizontal plane is spanned by the k_x and k_z axes. The vertical axis is the energy $E = E(k_x, \pi, k_z)$. (a) 2-band (cyan circle) and 4-band (red circle) touchings are observed at the P point. There appears other 2-band touchings (green circle) off the P point. (b)(c) An enlarged portion of the 2-band (4-band) touching indicates the emergence of (one) two Weyl cones at the P point.

quite simple. It contains three atoms represented by magenta, cyan and yellow spheres [Fig.2(b)]. Each color atom forms the body-center cubic lattice. We call it a tricolor cubic lattice. The Brillouin zone is shown in Fig.2(c). There are four high-symmetry points; $\Gamma(0, 0, 0)$, $P(\pi, \pi, \pi)$, $N(\pi, \pi, 0)$ and $H(2\pi, 0, 0)$. Additionally, there are important points named $\Delta(\pi, 0, 0)$, $G(3\pi/2, \pi/2, 0)$, $\Sigma(\pi/2, \pi/2, 0)$, $\Lambda(\pi/2, \pi/2, \pi/2)$, $F(3\pi/2, \pi/2, \pi/2)$, $D(\pi, \pi, \pi/2)$.

Model Hamiltonian: The main term of the lattice Hamiltonian is the hopping term along the bonds $\mathbf{d}_{ij} = \mathbf{r}_i - \mathbf{r}_j$ connecting a pair of the nearest neighbor sites i and j in the tricolor cubic lattice [Fig.2(a)]. We also introduce the spin-orbit interaction (SOI) preserving the cubic crystalline symmetry³⁰,

$$H_{\text{SO}} = i\lambda \sum_{\langle i, j \rangle} c_i^\dagger [\boldsymbol{\sigma} \cdot \mathbf{d}_{ij}] c_j, \quad (1)$$

with λ the coupling strength and $\boldsymbol{\sigma} = (\sigma_x, \sigma_y, \sigma_z)$ the Pauli matrix for the spin. The Hamiltonian has six bands due to the spin degrees of freedom. The 6-band Hamiltonian reads

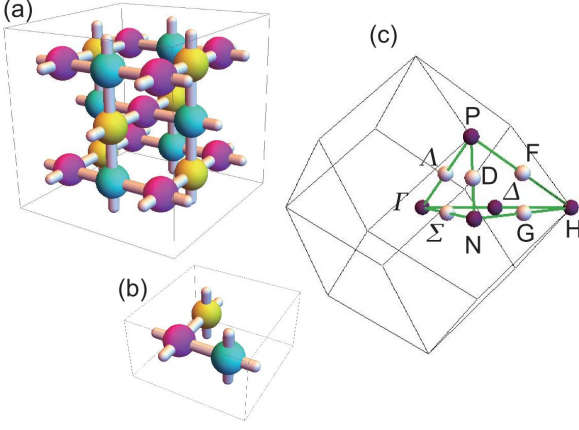


FIG. 2: **Lattice structure and the Brillouin zone.** (a) The lattice structure of a tricolor cubic lattice. (b) The unit cell contains three atoms, which are colored by magenta, cyan and yellow. Each colored atom forms the body-center cubic lattice. (c) The Brillouin zone and the high-symmetry points Γ , P , H , N , Δ . The green bold lines show the cut along the Γ - Δ - H - G - N - Σ - Γ - Λ - P - F - H - F - P - D - N line.

$\hat{H}_6 = \sum_{\mathbf{k}} c^\dagger(\mathbf{k}) H_6(\mathbf{k}) c(\mathbf{k})$ in the momentum space, where

$$H_6(\mathbf{k}) = I_2 \otimes \begin{pmatrix} 0 & f_x & f_y^* \\ f_x^* & 0 & f_z \\ f_y & f_z^* & 0 \end{pmatrix} + \sigma_x \otimes \begin{pmatrix} 0 & g_x & 0 \\ g_x^* & 0 & 0 \\ 0 & 0 & 0 \end{pmatrix} \\ + \sigma_y \otimes \begin{pmatrix} 0 & 0 & g_y^* \\ 0 & 0 & 0 \\ g_y & 0 & 0 \end{pmatrix} + \sigma_z \otimes \begin{pmatrix} 0 & 0 & 0 \\ 0 & 0 & g_z \\ 0 & g_z^* & 0 \end{pmatrix}, \quad (2)$$

with $f_\alpha = t \cos k_\alpha$, $g_\alpha = \lambda \sin k_\alpha$, $\alpha = x, y, z$, and the 2×2 unit matrix I_2 . We remark that the SOI is zero ($g_\alpha = 0$) at the high-symmetry points Γ , P , N , H and also at the Δ point.

Band structure: The energy spectrum is obtained by diagonalizing the Hamiltonian. We show the band structure along the line Γ - Δ - H - G - N - Σ - Γ - Λ - P - F - H - F - P - D - N in Fig.3 for typical values of the parameters t and λ . The 4-band and 2-band touchings are observed at various points in Fig.3(b). The high-symmetry point P is typical, around which we show the bird's eye's view of the band structure in Fig.1.

The 4-band touchings are protected by the cubic crystalline symmetry and the time-reversal symmetry. They occur at the high-symmetry points Γ , P , N , H and additionally at the Δ point. Hence, hereafter we count the point Δ as a member of the high-symmetry points. Let us explain how the 4-band touching emerges. As shown in Fig.3(a), in the absence of the SOI, the four-fold degeneracy is present due to the cubic crystalline symmetry at the high-symmetry points. Even by including the SOI, the bands never split at the time-reversal invariant momentum points, which implies the Kramers degeneracy. (In the present model this is realized since the SOI is zero at these points.) Consequently, the 4-fold degeneracy without the SOI yields the 4-band touching with the SOI at all the high-symmetry points [Fig.3(b)].

To explore these touchings analytically we diagonalize the

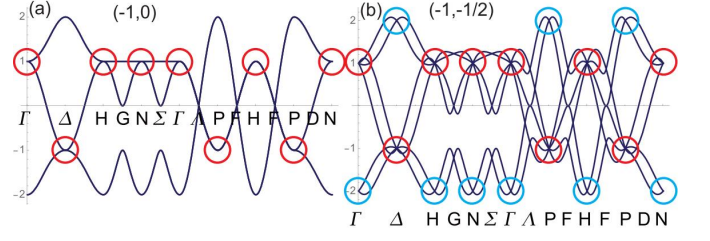


FIG. 3: **Band structures of the 6-band model.** The band structure along the Γ - Δ - H - G - N - Σ - Γ - Λ - P - F - H - F - P - D - N line for typical values of parameters (t, λ) as indicated in figures. (a) All energy bands are degenerate with respect to up and down spins when $\lambda = 0$. The 4-fold degenerate points are marked by magenta circles. (b) The spin degeneracy is resolved by the SOI ($\lambda \neq 0$) except for the high-symmetry points (indicated by circles) where the SOI vanishes. Pseudospin-3/2 fermions (red) and Weyl fermions (cyan) emerge at various points.

Hamiltonian by an unitary transformation U ,

$$U^{-1} H_6 U = \nu t \text{diag.}(2, 2, -1, -1, -1, -1), \quad (3)$$

at the high-symmetry points; $\nu = +$ for the Γ , N and H points and $\nu = -$ for the P and Δ points. The bands with the first two energies $2\nu t$ form a 2-band touching, while those with the four energies $-\nu t$ form a 4-band touching as in Fig.3(b).

4-band touching: First we construct the 4-band model by way of $H_4(\mathbf{k}) = P_4 U^{-1} H_6(\mathbf{k}) U P_4$, where U is fixed by (3) while P_4 is the projection operator from the 6×6 Hamiltonian to the 4×4 Hamiltonian containing the four bands with the eigen energies $-\nu t$. The 4-band Hamiltonian is derived up to the linear order of k_α as

$$\nu H_4 = -t \\ - \frac{\pi \lambda}{3} \begin{pmatrix} 0 & \eta \sqrt{3} k_z & 3 i k_y & \eta \sqrt{3} k_x \\ \eta \sqrt{3} k_z & -2 k_z & \eta \sqrt{3} k_x & 2 k_x - i k_y \\ -3 i k_y & \eta \sqrt{3} k_x & 0 & -\eta \sqrt{3} k_z \\ \eta \sqrt{3} k_x & 2 k_x + i k_y & -\eta \sqrt{3} k_z & 2 k_z \end{pmatrix}, \quad (4)$$

where $\eta = +$ for the Γ , P , N , H points and $\eta = -1$ for the Δ point. Here we have set the origin of the momentum $k_\alpha = 0$ at each high-symmetry point to investigate physics near the point. This Hamiltonian (4) is exactly diagonalizable,

$$E_j = \nu t \pm \frac{2j}{3} \lambda k, \quad k = |\mathbf{k}|, \quad (5)$$

which is independent of η , where $j = -3/2, -1/2, 1/2, 3/2$. The energy spectrum consists of two Weyl cones with velocities $\lambda/3$ and λ [Fig.1(b)].

Pseudospin 3/2 fermion: The energy eigenvalues (5) as well as the eigenfunctions are the same as those of the pseudospin-3/2 Weyl fermion defined by

$$H_4 = \nu t + \frac{2}{3} \lambda \mathbf{k} \cdot \mathbf{J}, \quad (6)$$

where \mathbf{J} is the pseudospin-3/2 operator. It implies that the Hamiltonian (4) is unitary equivalent to the system of the pseudospin-3/2 fermions.

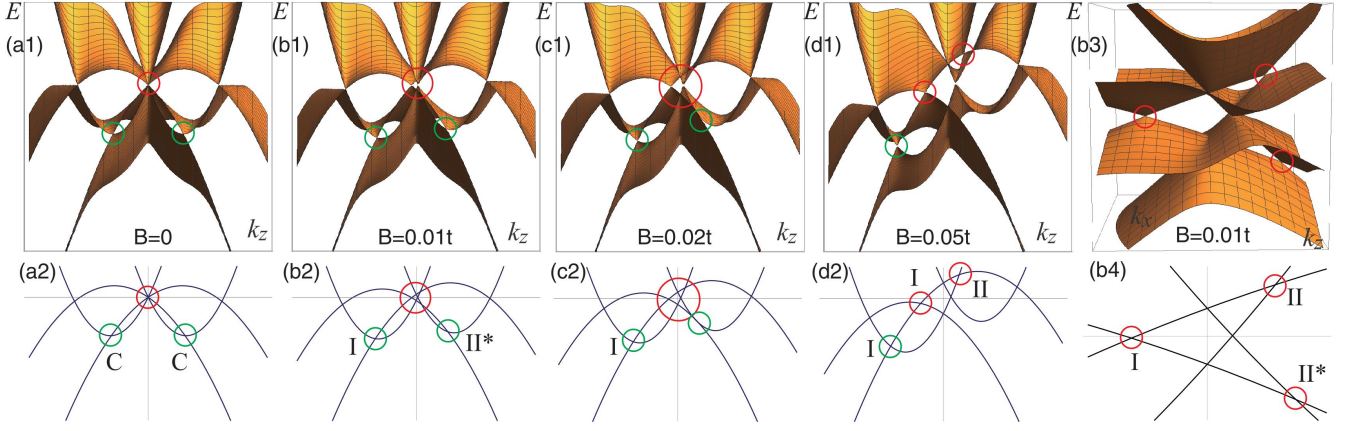


FIG. 4: **Band structures in the vicinity of the P point.** The horizontal axes are the k_z and k_x axes, while the vertical axis is the energy E . (a1)~(d1) The band structure without and with magnetic field B in the $[001]$ direction. The value of B is given in figures. 4-band touching (red circle) and two 2-band touchings (green) are observed. (a2)~(d2) 4-band and 2-band touchings occur along the k_z axis ($k_x = k_y = 0$). The cross sections of various surfaces are well approximated by parabolic curves. (b3) and (b4) show enlarged portions of the vicinity of the 4-band touching in (b1) and (b2), respectively. Symbols C, I and II stand for the critical, type-I and type-II Weyl points. The points indicated by Π^* are identical to those in Fig.5 and Fig.6. (b2) shows that the 4-band touching (red circle) is broken but the two 2-band touchings (green) are not. The critical Weyl points in (a2) turn out to be type-I and type-II Weyl points in (b2). See also Fig.5 for details. The pair of the type-II Weyl points (Π^*) in (c2) and (b4) are annihilated in (d2). See Fig.6 for details.

A comment is in order with respect to the pseudospin-3/2 fermion. It has already been proposed in antiperovskites, where the Hamiltonian is written as^{29,31}

$$H = m\tau_z + v_1\tau_x\mathbf{k} \cdot \mathbf{J} + v_2\tau_x\mathbf{k} \cdot \tilde{\mathbf{J}}. \quad (7)$$

It is an 8-band model due to the presence of another pseudospin degrees of freedom τ . Furthermore, this model has another operator $\tilde{\mathbf{J}}$ preserving the cubic symmetry, which introduces another velocity v_2 . In general, it is impossible to obtain the exact energy spectrum of this Hamiltonian.

Monopoles: With the use of the eigen function, the Berry curvature is explicitly calculated for each band as

$$\Omega_j = i\nabla \times \langle \psi_j | \nabla \psi_j \rangle = j \frac{\mathbf{k}}{k}, \quad (8)$$

where j labels the band with $j = -3/2, -1/2, 1/2, 3/2$. In deriving the formula we have used the fact $\frac{\partial \psi}{\partial r} = 0$. Since

$$\rho_j = \frac{1}{2\pi} \iiint \nabla \cdot \Omega_j = 2j = -3, -1, 1, 3, \quad (9)$$

the Berry curvature of the band indexed by j describes a monopole with the monopole charge $2j$.

Weyl semimetals: We may also construct the 2-band model by way of $H_2(\mathbf{k}) = P_2 U^{-1} H_6(\mathbf{k}) U P_2$, where P_2 is the projection operator from the 6×6 Hamiltonian to the 2×2 Hamiltonian containing the two bands with the eigen energies $2\nu t$ in (3). The low-energy 2-band model derived from this Hamiltonian describes Weyl fermions,

$$\nu H_2 = 2t + \frac{2}{3}\lambda(k_x\sigma_x - k_y\sigma_y - k_z\sigma_z). \quad (10)$$

We may verify the presence of monopole doublets ± 1 at the points Γ , N , H , and ∓ 1 at the points P , Δ , where the upper

(lower) component dictates the monopole charge of the upper (lower) band. It is remarkable that Weyl fermions emerge naturally in the present 3-dimensional tight-binding model. The Weyl semimetal is topologically protected as far as the 2-band touching is intact.

We note that there exist also 2-band touchings at the points G and Σ . However, since the effective theory is derived as

$$H = \pm(-t + \lambda k_z \sigma_z), \quad (11)$$

they do not describe Weyl semimetals.

Critical Weyl semimetals: 2-band touchings emerge also at points which have no conventional names. See points marked by two green circles in Fig.1(a) and Fig.4(a1). We study the band structure near the points. Since they locate on the k_z axis, we derive the energy spectrum of the Hamiltonian H_4 by setting $k_x = k_y = 0$. It is given up to the order of k_z^2 as

$$\nu E(0, 0, k_z) = -t \mp \lambda k_z + \frac{t}{2}k_z^2, \quad -t \mp \frac{\lambda}{3}k_z - \frac{t}{6}k_z^2. \quad (12)$$

We can check that these parabolic curves fit the results obtained by the 6 band tight-binding model very well. There are 2-band crossing points at $k_z = \pm\lambda/t$ with the energy $\pm(t + \lambda^2/2t)$: See Fig.4(a2). In the vicinity of these points, we derive the 2-band model with the use of $k'_z = k_z \mp \lambda/t$,

$$\begin{aligned} \nu H = & -t - \frac{\lambda^2}{2t} \mp \frac{1}{3}\lambda k'_z + \frac{t}{3}k'^2_z \\ & + \frac{\lambda}{\sqrt{3}} \left(-k_x\sigma_x + k_y\sigma_y + \frac{1}{\sqrt{3}}k'_z\sigma_z \right) \pm \frac{t}{3}k'^2_z\sigma_z. \end{aligned} \quad (13)$$

The energy spectrum along the k_z axis is given by

$$\nu E(0, 0, k'_z) = -t - \frac{\lambda^2}{2t} + \frac{t}{2}k'^2_z, \quad -t - \frac{\lambda^2}{2t} \mp \frac{2}{3}\lambda k'_z - \frac{t}{6}k'^2_z. \quad (14)$$

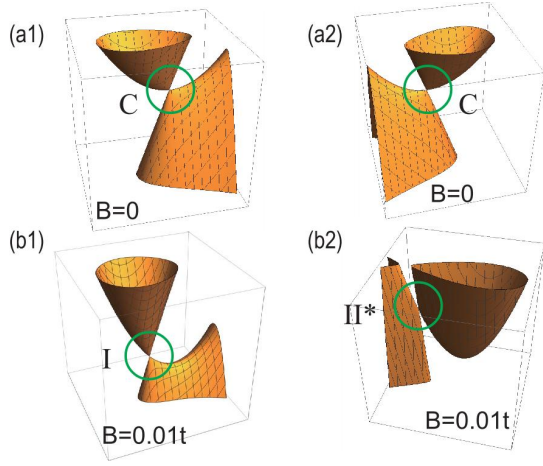


FIG. 5: **Transition from the critical Weyl fermions to the type-I and type-II Weyl fermions.** (a1),(a2) Critical Weyl points. (b1) Type-I Weyl point. (b2) Type-II Weyl point. They represent bird's eye's views of the corresponding points in Fig.4(a2) and (b2).

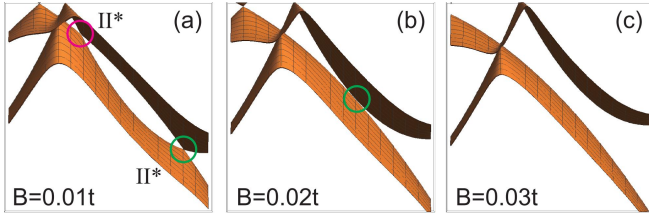


FIG. 6: **Pair-annihilation of two type-II Weyl fermions.** (a) shows a bird's eye's view of the type-II points marked II* in Fig.4(b2) and in Fig.4(b4). (b) These two Weyl fermions merge at a critical magnetic field as in Fig.4(c2). (c) They are annihilated beyond the critical field.

Interestingly, the linear order of k'_z is absent in the second energy spectrum. Consequently, they are a critical Weyl semimetals between the type I and II Weyl semimetals.

Magnetic-field-induced type-II Weyl semimetals: We apply external magnetic field ($B \neq 0$) in the [001] direction. The Hamiltonian is given by adding the term $B\sigma_z \otimes I_3$ to the Hamiltonian (2), where I_3 is the 3×3 unit matrix. There occurs the Zeeman split in the band structure as in Fig.4.

With respect to the 2-band touching (Weyl point), the only effect of the magnetic field is adding the Zeeman term $B\sigma_z$ to the Hamiltonian (10). It results in a shift of the Weyl point in the z direction, but the gap never opens.

On the other hand, the 4-band touching is broken under the magnetic field. This is because it is protected by the time-reversal symmetry and the cubic symmetry.

Type-II Weyl fermions are produced in two different ways as the magnetic field is introduced. (i) First, as we remarked just in above, there exist critical Weyl points in the vicinity of the 4-band touching point [Fig.4(a) and Fig.5(a)]. They are turned into the type-I and type-II Weyl points [4(b) and Fig.5(b)]. (ii) Second, as the 4-point touching is broken, there appear six 2-point touchings in general as in Fig.4(b4), among which we find type-II Weyl points.

We discuss the case (i): See Fig.5. We study how the critical Weyl fermions are modified under magnetic field. The crossing points are given by $k_z = \pm (\lambda + \sqrt{\lambda^2 + 12Bt}) / 2t$. In the linear order of B , the additional term to the 2-band model (13) is

$$\nu H_B = B \left(\pm 1 + \frac{t}{\lambda} k'_z - \frac{2t}{\lambda} k'_z \sigma_z \right). \quad (15)$$

It transforms the two critical Weyl fermions into the type-I and type-II Weyl fermions.

Next we discuss the case (ii): See Fig.4(b3). In the 4-band linear model, the energy spectrum along the k_z axis is given by $-\nu E = t \pm (\lambda k_z - B)$, $t \pm (\frac{1}{3}\lambda k_z - B)$. There are 2-band crossings at $k_z = 3B/\lambda$. In the vicinity of this point, the 2-band model is given by

$$H = \pm [-t + 2B - \frac{2}{3}\lambda k'_z - \frac{\lambda}{\sqrt{3}}(k_x \sigma_x - k_y \sigma_y - \frac{1}{\sqrt{3}}k'_z \sigma_z)] \quad (16)$$

with the energy spectrum

$$E = \pm \left(-t + 2B - \frac{2}{3}\lambda k'_z \pm \frac{1}{3}\lambda \sqrt{3k_x^2 + 3k_y^2 + k_z'^2} \right). \quad (17)$$

Since the tilt of the Weyl cone is larger than the velocity of the Weyl cone, they are type-II Weyl points.

We have mentioned the emergence of type-II Weyl points in two different ways. Interestingly they are pair annihilated at $B = \pm \lambda^2 / 12t$ and disappear for $|B| > \lambda^2 / 12t$, as shown in Fig.6(b) and Fig.6(c), respectively.

The author is very much grateful to N. Nagaosa for many helpful discussions on the subject. He thanks the support by the Grants-in-Aid for Scientific Research from MEXT KAKENHI (Grant Nos. JP25400317 and JP15H05854).

¹ P. Hosur, X.L. Qi, C. R. Physique 14, 857 (2013)
² S. Murakami, New J. Phys. 9, 356 (2007)
³ A. A. Soluyanov, D. Gresch, Z. Wang, Q.S. Wu, M. Troyer, X. Dai and B. Andrei Bernevig, Nature, 527, 495 (2015)
⁴ Y. Sun, et.al., Phys. Rev. B 92, 161107 (2015)
⁵ Z. Wang, et.al., Phys. Rev. Lett. 117, 056805 (2016)
⁶ J. H. Pixley, D. A. Huse, S. Das Sarma, Phys. Rev. X 6, 021042 (2016)
⁷ T. E. O'Brien, M. Diez, C. W. J. Beenakker, Phys. Rev. Lett. 116,

236401 (2016)
⁸ Z.-M. Yu, Y. Yao, S. A. Yang, Phys. Rev. Lett. 117, 077202 (2016)
⁹ A. Tamai, et.al., Phys. Rev. X 6, 031021 (2016)
¹⁰ S. Tchoumakov, M. Civelli, M. O. Goerbig, Phys. Rev. Lett. 117, 086402 (2016)
¹¹ C.-K. Chan, Y.-T. Oh, J. H. Han, P. A. Lee, Phys. Rev. B 94, 121106(R) (2016)
¹² M. Udagawa and E. J. Bergholtz, Phys. Rev. Lett. 117, 086401 (2016)

- ¹³ L. Huang, et.al., cond-mat/arXiv:1603.06482
- ¹⁴ K. Deng, et.al., cond-mat/arXiv:1603.08508 (Nature Physics in press)
- ¹⁵ J. Jing, et.al., cond-mat/arXiv:1604.00139
- ¹⁶ A. Liang, cond-mat/arXiv:1604.01706
- ¹⁷ N. Xu, cond-mat/arXiv:1604.02116
- ¹⁸ S.Y. Xu, et.al., cond-mat/arXiv:1603.07318
- ¹⁹ C. Wang, et.al., cond-mat/arXiv:1604.04218
- ²⁰ Y. Wu, et.al., cond-mat/arXiv:1604.05176
- ²¹ B. Feng, et.al., cond-mat/arXiv:1606.00085
- ²² Y. Wang, et.al., cond-mat/arXiv:1608.05003 (Nat. Com. in press)
- ²³ S. Khim, et.al., cond-mat/arXiv:1604.03380
- ²⁴ M. Yan, et.al., cond-mat/arXiv:1607.03643
- ²⁵ D. Chen, et.al., cond-mat/arXiv:1604.05798
- ²⁶ B. Bradlyn, *et al*, Science (2016)
- ²⁷ G. Chang, et.al., cond-mat/arXiv:1605.06831
- ²⁸ B. J. Wieder, Y. Kim, A.M. Rappe, and C.L. Kane, Phys. Rev. Lett. 116, 186402 (2016)
- ²⁹ T. H. Hsieh, J. Liu and L. Fu, Phys. Rev. B 90, 08112(R) (2014)
- ³⁰ M. Ezawa, New Journal of Physics 16, 065015 (2014)
- ³¹ H. Isobe and L. Fu, cond-mat/arXiv:1604.01805.